J. Fluid Mech. (1988) *vol.* 188, *pp.* 509–527
Printed in Great Britain

Oscillatory flow and mass transport in a curved tube

By DAVID M. ECKMANN AND JAMES B. GROTBERG

Biomedical Engineering Department, The Technological Institute, Northwestern University, Evanston, IL 60208, USA *and* Department of Anesthesia, Northwestern University Medical School, Chicago, IL 60611, USA

(Received 31 March 1987 and in revised form 3 September 1987)

Transport of soluble material is analysed for volume-cycled oscillatory flow in a curved tube. The equations of motion are solved using a regular perturbation method for small ratio of tube radius to radius of curvature and order unity amplitude over a range of the Womersley parameter. The transport equation is similarly solved by a regular perturbation scheme where uniform steady end concentrations and no wall flux are assumed. The time-average axial transport of solute is calculated. There is substantial modification of transport compared to the straight-tube case and the results are interpreted with respect to pulmonary gas exchange.

1. Introduction

The delivery and removal of mass (oxygen, carbon dioxide, anaesthetics, drugs, aerosols, toxins) and heat through the lung are primary phenomena of normal respiration. They are also the main thrust of design for conventional and high-frequency ventilators (Bohn *et al.* 1980; Butler *et al.* 1980), incubators and nebulizers, as well as the result of chemical pollution in the air, both chronic and disaster related. The sequence of physical events leading to the exchange of mass and heat between the lung and the environment depends on convection and diffusion in an oscillatory flow. The basic geometric unit which influences the fluid mechanics and transport characteristics is the airway bifurcation joining the parent to the two daughter airways. A theoretical analysis of oscillating flow in a tube bifurcation would be difficult to attack directly. However, we know from the geometry of a bifurcation that it possesses characteristics of both taper and axial curvature through the region, as well as flow division. So a reasonable approach is to examine these effects individually as a start towards understanding the total phenomenon.

The effects of taper were investigated both in theory by Grotberg (1984) and Godleski & Grotberg (1987) and by experiment by Gaver & Grotberg (1986), and were found to have an important influence on transport of soluble and insoluble contaminants. In a tapered tube, the streamlines are curved, having axial and radial velocity components. Solute is convected along streamlines, but crosses them by either radial or axial diffusion. This leads to more complicated transport behaviour than straight-tube oscillating flows where only radial diffusion leads to crossing of parallel streamlines. Depending on the values of α, the Womersley parameter, and A, the amplitude parameter, the transport predicted for tapered tubes can be greater or less than the corresponding straight-tube case as shown by Godleski & Grotberg (1987). For insoluble contaminants, which rely solely on convective transport, the experiments of Haselton & Scherer (1982) show that volume-cycled oscillating flow

in a model bifurcation leads to bidirectional steady streaming. Those data are consistent with the predictions by Grotberg (1984) and the experiments of Gaver & Grotberg (1986), who studied oscillatory flow in a tapered channel.

Theoretical investigations of dispersion for unidirectional flows in straight tubes have been made by Taylor (1953), for pulsatile flows in curved tubes by Blennerhasset (1976) and for oscillatory flows in straight tubes by Chatwin (1975) and Watson (1983). The predictions by Watson are consistent with gas exchange experiments in a straight tube by Joshi *et al.* (1983), a companion paper. However, similar experiments were conducted by Paloski, Slosberg & Kamm (1987) for a branching network of tubes and the transport rates were found to be much higher than the predictions of Watson's single, straight-tube theory. Apparently the presence of bifurcations in the network can enhance axial exchange, which raises the importance of an enquiry into the effects of taper, curvature, and flow division.

Laminar dispersion in steady flows in uniformly curved tubes has been the subject of several theoretical and experimental studies. Longitudinal dispersion for steady laminar flow in helical tubes of small pitch decreases from that in straight tubes as shown by the analytical solution of Erdogan & Chatwin (1967) and the numerical analysis of Janssen (1976). Most recently, Johnson & Kamm (1986) used Monte Carlo and spectral models to calculate dispersion in such a geometry. Their results also show disenhancement of longitudinal transport for increasing curvature. Experimental evidence further suggests that curvature reduces longitudinal mass transport in tubes. Measurements made by Van Den Berg & Deelder (1979) show that for small curvature and small diffusion, there is no significant difference between mass transport in straight tubes and helical coils. They further show that as diffusion and curvature increase, axial dispersion in the helical coils decreases as compared to axial dispersion in straight tubes.

Nigam & Vasudeva (1976) investigated experimentally the effect of small pulsations on mass transport in laminar flow in curved tubes and found that transport could be higher, equal to or less than that for steady flow, dependent on the experimental conditions. This suggests that the oscillatory component has a striking influence on the transport characteristics and should be studied independently.

Prior to solving the transport problem it is necessary to find the velocity field for an oscillatory flow in a curved tube. The equations of momentum and conservation of mass, given below, have been used by many authors to calculate fluid motions in curved tubes. Mullin & Greated (1980) expand the velocity field in integral powers of δ, the ratio of tube radius, a, to radius of axial curvature, R. To simplify the equations and allow some progress, they use the stream function for a straight circular cylinder. This technique neglects some terms of $O(\delta)$ which we will show to be important in the transport problem we address here, so we cannot follow their method of solution. Berger, Talbot & Yao (1983), however, expand in powers of $\delta^{\frac{1}{2}}$ which brings in convective acceleration effects sooner, since they are stronger. However, the effects of curvature are relatively weak in this solution, giving secondary motions of $O(\delta)$ compared to the axial flow. Lyne (1970), whose scaling we have followed, utilizes the same stream function as Mullin & Greated. He considers solutions of the equations in the limit as $\delta \to 0$. If we let Lyne's velocity scale, $\bar{W} = \omega d$, where $d = V_T/(\pi a^2)$ is the stroke distance and V_T is the tidal volume, then his solution is restricted to $A \gg 1$, where $A = d/a$, such that δA^2 is $O(1)$. This limit is similar to one considered by Smith (1975). The nonlinear inertia terms cause a perturbation to the solution before the first-order correction in δ. Now convective

acceleration is important at leading order in the Navier–Stokes equations. For slightly curved tubes this requires large stroke distance, so that a particle moving an axial distance $d\delta^{\frac{1}{2}}$ experiences an $O(1)$ centrifugal force. However, we prefer to keep $A \approx O(1)$, since this is an important parameter regime in a practical sense when considering the physiological application. Thus, as in Lyne (1970), nonlinear inertia effects are analysed as a perturbation to the flow; in fact, when $A \approx O(1)$, the nonlinear inertia is an $O(\delta)$ perturbation to the solution so that techniques as used by Mullin & Greated (1980) are appropriate when all $O(\delta)$ terms are considered.

2. Problem formulation: velocity field

Consider a section of a torus shown in figure 1 as representative of the curved portion of an airway bifurcation. The fluid oscillates along the axial coordinate, $\overset{*}{s}$, and we expect secondary flows in the $(\overset{*}{r}, \psi)$-plane. The axial radius of curvature is R and the tube wall boundary is described by $\overset{*}{r} = a$. The fluid has density ρ and kinematic viscosity ν. Let the velocity vector be $\overset{*}{\boldsymbol{u}} = (\overset{*}{u}, \overset{*}{v}, \overset{*}{w})$ whose components are in the $(\overset{*}{r}, \psi, \overset{*}{s})$-directions, respectively. The momentum conservation is given by the Navier–Stokes equations in toroidal coordinates. Assuming fully developed flow, such that $\partial \boldsymbol{u}/\partial s = \boldsymbol{0}$, the dimensionless forms of the equations are

$$u_\tau + \delta A^2\left[uu_r + \frac{v}{r}u_\psi - \frac{v^2}{r}\right] - \frac{(w^2\cos\psi)}{h} = -p_r - \alpha^{-2}\left[\frac{1/r\,\partial}{\partial\psi} - \frac{(\delta\sin\psi)}{h}\right]\left[v_r + \frac{v}{r} - \frac{1}{r}u_\psi\right], \tag{2.1a}$$

$$v_\tau + \delta A^2\left[uv_r + \frac{v}{r}v_\psi + \frac{uv}{r}\right] + \frac{(w^2\sin\psi)}{h} = -\frac{1}{r}p_\psi - \alpha^{-2}\left[\frac{\partial}{\partial r} + \frac{(\delta\cos\psi)}{h}\right]\left[v_r + \frac{v}{r} - \frac{1}{r}u_\psi\right], \tag{2.1b}$$

$$w_\tau + \delta A^2\left[uw_r + \frac{v}{r}w_\psi + \frac{(uw\delta\cos\psi)}{h} - \frac{(vw\delta\sin\psi)}{h}\right] = -\frac{p_s}{h} + \alpha^{-2}\left[\left(\frac{\partial}{\partial r} + \frac{1}{r}\right)\left(w_r + \frac{(w\delta\cos\psi)}{h}\right) + \frac{1}{r}\left(\frac{1}{r}w_\psi - \frac{(w\delta\sin\psi)}{h}{}_\psi\right)\right], \tag{2.1c}$$

and the conservation of mass for an incompressible fluid is given by:

$$u_r + \frac{u}{r} + \frac{u\delta\cos\psi}{h} + \frac{1}{r}u_\psi - \frac{v\delta\sin\psi}{h} = 0. \tag{2.2}$$

Subscripts imply partial differentiation with respect to the indicated independent variable, and the symbol $h = 1 + \delta r\cos\psi$.

Fluid motion for this problem is driven by an oscillatory pressure gradient such that a fixed volume of fluid, V_T, passes through any cross-section in one half-cycle. We define the angular frequency of oscillation as ω and the stroke distance as $d = V_T/\pi a^2$, which represents the typical distance a fluid particle moves in a half cycle. The typical axial velocity scales with $U = \omega d$. Lateral velocities, however, depend on the centrifugal acceleration of a particle, given by U^2/R. Thus an appropriate velocity scale for lateral velocities is $U^2/\omega R = \delta A U$.

The dimensionless variables are defined by the following,

$$u = \frac{\overset{*}{u}}{\delta A U}, \quad v = \frac{\overset{*}{v}}{\delta A U}, \quad w = \frac{\overset{*}{w}}{U}, \quad p = \frac{\overset{*}{p}}{\delta\rho U^2}, \quad \tau = \omega\overset{*}{t}, \quad r = \frac{\overset{*}{r}}{a}, \quad s = \frac{\overset{*}{s}}{a}. \tag{2.3}$$

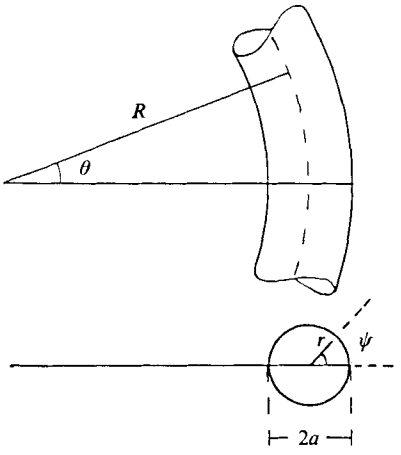

FIGURE 1. The toroidal coordinate system.

The three non-dimensional parameters arising from these scalings appear in the above equations and are: the amplitude parameter $A = d/a$, the ratio of stroke distance to pipe radius; the Womersley parameter, $\alpha = a(\omega/\nu)^{\frac{1}{2}}$, the ratio of pipe radius to Stokes layer thickness; and $\delta = a/R$, the curvature parameter.

The boundary conditions at the wall are no slip and no penetration,

$$u = 0, \quad v = 0, \quad w = 0 \quad \text{at } r = 1, \tag{2.4a, b, c}$$

and the axial velocity is constrained to a fixed tidal volume, V_T, given by the integral constraint:

$$\int_0^{2\pi} \int_0^1 wr \, dr \, d\psi = \tfrac{1}{4}\pi e^{i\tau} + \text{c.c.}, \tag{2.5}$$

where c.c. denotes complex conjugate. The constant $\frac{1}{4}\pi$ is selected out of convenience since it will allow direct comparison of our results with those of Godleski & Grotberg (1987) and Watson (1983).

3. Method of solution

It is convenient to eliminate pressure as a variable in the u and v momentum equations by defining the stream function χ such that

$$u = \frac{1}{r}\chi_\psi - \frac{\delta \sin\psi}{h}\chi, \tag{3.1a}$$

$$v = -\chi_r - \frac{\delta \cos\psi}{h}\chi, \tag{3.1b}$$

which satisfy (2.2) exactly. The addition of the second terms in the definitions of u and v makes this treatment of the problem more rigorous than previous investigations of Lyne (1970) and Mullin & Greated (1980). Their choice of stream function consists of only the first terms for u and v which satisfy continuity for a straight, rather than a curved pipe. Substituting our definitions of u and v into equations (2.1a–c) reduces

the velocity field to a system of two equations in two unknowns (w, χ). The boundary conditions for this system are

$$w = 0 \quad \text{at } r = 1, \tag{3.2a}$$

$$\chi = 0, \quad \chi_r = 0 \quad \text{at } r = 1, \tag{3.2b, c}$$

$$\chi, w \text{ bounded at } r = 0, \tag{3.2d, e}$$

$$\text{vorticity bounded at } r = 0. \tag{3.2f}$$

The anatomy of the human lung is such that the value of δ ranges from approximately 0.1 to 0.3, so it is appropriate to investigate gently curving tubes, $\delta \ll 1$. This suggests linearizing the equations of fluid motion by using a regular perturbation scheme in the small parameter δ. For small axial fluid displacements, we expand the axial velocity component and the stream function, w and χ, and the pressure, p, in powers of δ, as shown:

$$w(r, \psi, \tau) = w_0(r, \psi, \tau) + \delta w_1(r, \psi, \tau) + \delta^2 w_2(r, \psi, \tau) + O(\delta^3), \tag{3.3a}$$

$$\chi(r, \psi, \tau) = \chi_0(r, \psi, \tau) + \delta \chi_1(r, \psi, \tau) + O(\delta^2), \tag{3.3b}$$

$$p(r, \psi, \tau, s) = p_0(r, \psi, \tau, s) + \delta p_1(r, \psi, \tau, s) + \delta^2 p_2(r, \psi, \tau, s) + O(\delta^3). \tag{3.3c}$$

Inserting these expansions into the axial momentum and vorticity equations and equating to zero the coefficient of each power of δ gives a set of linear boundary-value problems at successive orders of δ. The leading-order solution is:

$$p_{0s} = p_0 \, e^{i\tau} + \text{c.c.} = \frac{i J_0(\sigma)}{4 J_2(\sigma)} e^{i\tau} + \text{c.c.} \tag{3.4a}$$

$$w_0 = W_0(r) \, e^{i\tau} + \text{c.c.} = i P_0 \left[1 - \frac{J_0(\sigma r)}{J_0(\sigma)} \right] e^{i\tau} + \text{c.c.} \tag{3.4b}$$

In these equations, J_n is the order n Bessel function of the first kind and $\sigma = \alpha i^{\frac{3}{2}}$.

The solution to the leading-order stream-function problem is not written explicitly. The inhomogeneous forcing term in the equation for χ_0 has steady and $2i\tau$-dependent components. We seek a solution to χ_0 which is the sum of a steady part, $\chi_0^{(s)}$, and a periodic part, $\chi_0^{(p)}$. By separating variables and employing the technique of variation of parameters, $\chi_0^{(s)}$ is determined to be

$$\chi_0^{(s)} = g_1(r) \sin \psi, \tag{3.5}$$

where the function $g_1(r)$ is given in integral form,

$$g_1(r) = b_1 r + \frac{c_1 r^3}{8} + \frac{r^3}{16} \int_0^r f_1(z) \, dz - \frac{1}{16 r} \int_0^r z^4 f_1(z) \, dz + \tfrac{1}{4} r \int_0^r z^2 \ln z \, f_1(z) \, dz - \tfrac{1}{4} r \ln r \int_0^r z^2 f_1(z) \, dz, \tag{3.6}$$

and $f_1(r) = -2\alpha^2 W_0 \bar{W}_{0r} + \text{c.c.}$ The constants b_1 and c_1 are determined from $O(1)$ boundary conditions, and the superscript bar denotes complex conjugate.

A similar technique is used to determine the periodic component of the stream function. The solution is of the form

$$\chi_0^{(p)} = g_2(r) \, e^{2i\tau} \sin \psi + \text{c.c.} \tag{3.7}$$

where

$$g_2(r) = [e_1 + F_1(\kappa, 2^{\frac{1}{2}}\sigma, 1)] \, J_1(2^{\frac{1}{2}}\sigma) + F_2(\kappa, 2^{\frac{1}{2}}\sigma, 1) \, Y_1(2^{\frac{1}{2}}\sigma r), \tag{3.8}$$

such that $F_1(Q,R,N)$ and $F_2(Q,R,N)$ are the coefficients of the particular solution determined by variation of parameters and are defined as

$$F_1(Q,S,T) = -\tfrac{1}{2}\pi \int_0^r Q Y_T(Sz)\, z\, dz, \tag{3.9a}$$

$$F_2(Q,S,T) = \tfrac{1}{2}\pi \int_0^r Q J_T(Sz)\, z\, dz, \tag{3.9b}$$

and

$$\kappa(r) = d_1 r + \frac{d_2}{r} + \tfrac{1}{2} r \int_0^r G(z)\, dz - \frac{1}{2r}\int_0^r z^2 G(z)\, dz, \tag{3.10}$$

for $G(r) = W_0 W_{0r}$. The constants d_1, d_2 and e_1 are determined from the $O(1)$ boundary conditions.

The solutions to the higher-order equations are found in identical manner. Since the leading-order axial velocity component satisfies the volume constraint, we find that this requires that, at all subsequent $O(\delta^n)$, $P_{ns} = 0$ for $n \geqslant 1$. Subsequently, the forcing terms of the $O(\delta)$ axial velocity equation can be written as

$$[H_1(r)\, e^{i\tau} + H_2(r)\, e^{3i\tau}] \cos\psi. \tag{3.11}$$

The solution of w_1 is of the form

$$w_1 = h_1(r)\, e^{i\tau} \cos\psi + h_2(r)\, e^{3i\tau} \cos\psi + \text{c.c.} \tag{3.12}$$

where

$$h_1(r) = [k_1 + F_1(H_1, \sigma, 1)]\, J_1(\sigma r) + F_2(H_1, \sigma, 1)\, Y_1(\sigma r), \tag{3.13a}$$

$$h_2(r) = [k_2 + F_1(H_2, 3^{\frac{1}{2}}\sigma, 1)]\, J_1(3^{\frac{1}{2}}\sigma r) + F_2(H_2, 3^{\frac{1}{2}}\sigma, 1)\, Y_1(3^{\frac{1}{2}}\sigma r), \tag{3.13b}$$

and k_1, k_2 are constants determined from the boundary condition at $O(\delta)$.

Looking ahead to the mass flux calculation, we find that the important contributions from the velocity field, which we will need to solve the convection–diffusion equation and determine the effective diffusivity, are the ψ-independent component of w_2 which has $e^{i\tau}$-periodicity, and the steady component of χ_1.

The $O(\delta)$ vorticity equation suggests the form for the first correction to the stream function

$$\chi_1 = [\zeta_1(r) + (\zeta_2(r)\, e^{2i\tau} + \zeta_3(r)\, e^{4i\tau} + \text{c.c.})] \sin 2\psi. \tag{3.14}$$

In this study we only determine $\zeta_1(r)$, the radial dependence of the steady stream function, by employing the same techniques used to find χ_0. The steady forcing terms of the $O(\delta)$ vorticity equation can be combined as a single function, $I(r)\sin 2\psi$. Then $\zeta_1(r)$ is given by

$$\zeta_1(r) = m_1 r^2 + \tfrac{1}{12} m_2 r^4 + \tfrac{1}{46} r^4 \int_0^r \frac{I(z)}{z}\, dz - \tfrac{1}{16} r^2 \int_0^r z I(z)\, dz + \frac{1}{16}\int_0^r z^3 I(z)\, dz - \frac{1}{48 r^2}\int_0^r z^5 I(z)\, dz, \tag{3.15}$$

where m_1 and m_2 are constants determined by the boundary conditions at $O(\delta)$.

Similarly, upon substitution of the expansions the $O(\delta^2)$ axial velocity equation shows forcing terms dependent on $\sin 2\psi$, $\cos 2\psi$, and independent of ψ. The suggested solution is of the form

$$\begin{aligned} w_2 = {} & [\lambda_1(r)\, e^{i\tau} + \lambda_2(r)\, e^{3i\tau} + \lambda_3(r)\, e^{5i\tau} + \text{c.c.}] \\ & + [\beta_1(r)\, e^{i\tau} + \beta_2(r)\, e^{3i\tau} + \beta_3(r)\, e^{5i\tau} + \text{c.c.}] \sin 2\psi \\ & + [\xi_1(r)\, e^{i\tau} + \xi_2(r)\, e^{3i\tau} + \xi_3(r)\, e^{5i\tau} + \text{c.c.}] \cos 2\psi. \end{aligned} \tag{3.16}$$

Our interest is in finding $\lambda_1(r)$ in this work, since it is a necessary component of the mass flux integral to be determined. We calculate $\lambda_1(r)$ subject to the $O(\delta^2)$ boundary conditions in the same manner used to solve the $O(\delta)$ axial velocity equation. The radial dependence of the $e^{i\tau}$-periodic, ψ-independent forcing terms of the $O(\delta^2)$ axial velocity equation can be combined into a single function, $\theta(r)$. Then $\lambda_1(r)$ is determined to be

$$\lambda_1(r) = [n_1 + F_1(\theta, \sigma, 0)] J_0(\sigma r) + F_2(\theta, \sigma, 0)\, Y_0(\sigma r), \tag{3.17}$$

where n_1 is determined from no-slip boundary condition at $r = 1$.

4. Results: velocity field

The computed axial velocity profiles are shown to $O(\delta)$ in figure 2 (a, b) at several different phases in the cycle. Note that the quasi-steady low α case, plotted in figure 2(a), has the characteristic parabolic shape which is distorted slightly toward the outside of the tube. This is similar to the results for steady flow in a curved tube, where the centrifugal effects cause a slight outward distortion of the parabolic profile. As α increases we see the development of the viscous boundary layer (figure 2b), with the velocity higher near the inside wall than at the outside wall. The plots presented are for the velocities in the plane of curvature, where the unsteady centrifuging has its greatest effect. These results correlate well with the experiments of Bertelsen & Thorsen (1982), the theory and experiments of Mullin & Greated (1980) and the numerical analysis of Yamane *et al.* (1985). Careful analysis for $\alpha \gg 1$ of the individual non-homogeneous forcing terms in the $O(\delta)$ axial velocity equation shows that the dominant balance is the axial pressure gradient and unsteady acceleration in the core. Since $p_{ns} = 0$ for all $n \geqslant 1$, the leading-order pressure drives flow at all subsequent orders of δ. In the term $(1/h)\,(\partial p/\partial s)$ of equation (2.1c), when h^{-1} is properly expanded in powers of δ, the pressure gradient p_{0s} influences all orders of δ, where its effects are modified by this geometrical coefficient. This explains why the velocities are higher on the inside than on the outside to the degree that we find. The distance along the inside of the tube is shorter than the distance along the outside; therefore the axial pressure gradient must be higher along the inside than the outside of the tube.

The solution to the $O(\delta)$ axial velocity depends on the forcing term $p_{0s} r \cos\psi$. From our coordinate system we see that $\psi = 0$ corresponds to the outer wall, meaning that we add a radial-dependent term to the leading-order solution in the outer half of the tube, while $\psi = \pi$ corresponds to the inner wall, meaning that we subtract that same radial-dependent term from the leading-order solution in the inner half of the tube. Thus there is a decrease in the outer-wall velocity and an increase in the inner-wall velocity for large enough α, since the $O(\delta)$ radial-dependence of the axial velocity, driven by the axial pressure gradient, is negative. The corresponding increase and decrease are of equal magnitude. We would expect the magnitudes to differ at $O(\delta^2)$.

When we allow α to increase above 10 we begin to see appreciable differences in the results generated from the asymptotic equations of previous authors and our own work. This is shown in figure 3, where the axial velocity profiles for $\tau = 0$, $A = 1$, $\delta = 0.3$ and $\alpha = 15$ are plotted for the straight tube, this work and the volume-cycled form of the equations used by Mullin & Greated (1980). The variation is particularly accentuated at this instant in time. Since we are interested in investigating the mass transport characteristics of HFV (large α), it does show the importance of keeping all

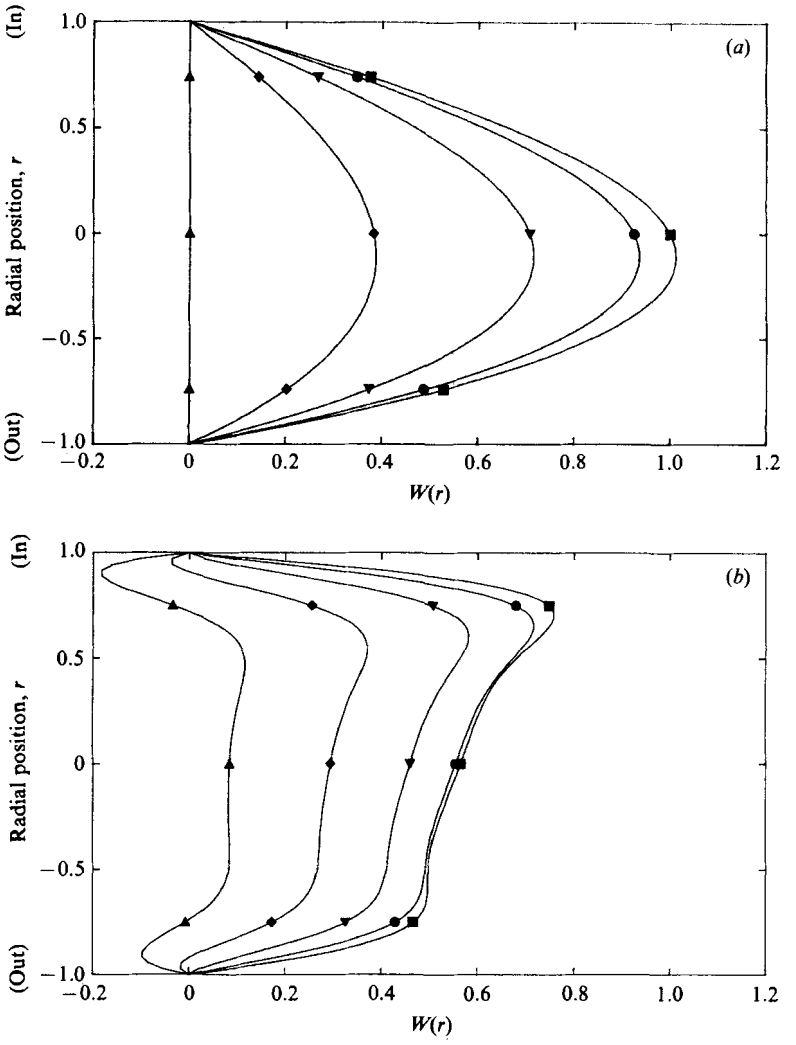

FIGURE 2. Axial velocity profile in the plane of curvature as a function of r. $A = 1.0$, $\delta = 0.3$. Phases shown are ■, $\tau = 0$; ●, $\tau = \frac{1}{8}\pi$; ▼, $\tau = \frac{1}{4}\pi$; ◆, $\tau = \frac{3}{8}\pi$; ▲, $\tau = \frac{1}{2}\pi$. (*a*) $\alpha = 0.2$; (*b*) $\alpha = 10.0$.

of the $O(\delta)$ information when solving the equations of motion. We may otherwise lose details of the flow which have an important bearing on the transport phenomena and the predictive value of the model.

The steady cross-sectional streaming is depicted in figure 4(*a–c*), where closed contours of constant $\chi^{(s)}$ to $O(\delta)$ are drawn. For $\alpha = 1$, figure 4(*a*) shows two cells as predicted by Lyne (1970). As we increase α to 10, these two cells begin to squeeze toward the top and bottom of the tube (figure 4*b*). This means that the viscous effects of the fluid are being felt near the tube boundary. This is also evident from the development of the boundary layer seen in the axial profile for the same value of α. When α is increased to 15 we observe in figure 4(*c*) the appearance of a second set of cells, with opposite vorticity, near the centre of the tube. These vew cells arise from a pressure gradient which is no longer opposed by viscous forces in the core region. The two original cells are confined to a thinner layer near the wall.

The cross-sectional steady streaming phenomena have been predicted by previous

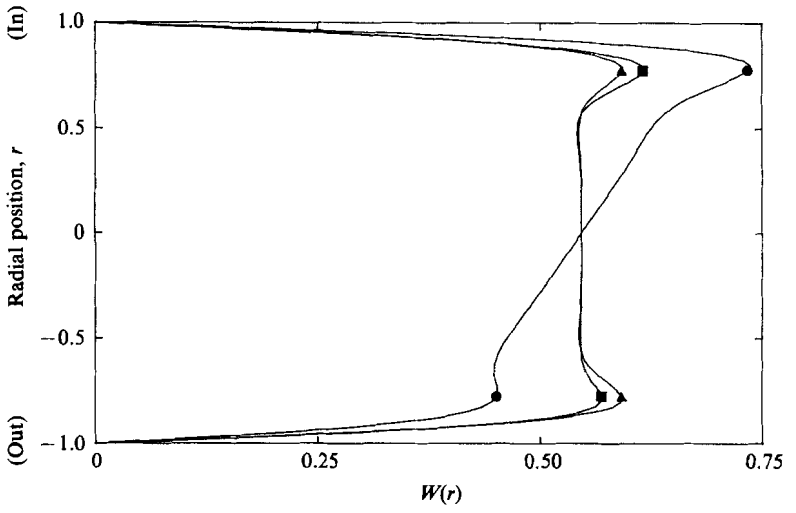

FIGURE 3. Axial velocity profile in the plane of curvature as a function of r. $A = 1.0$, $\alpha = 15.0$, $\tau = 0$. Profiles shown are for ▲, $\delta = 0$; ■, $\delta = 0.3$ (Mullin & Greated 1980), ●, $\delta = 0.3$ (our results).

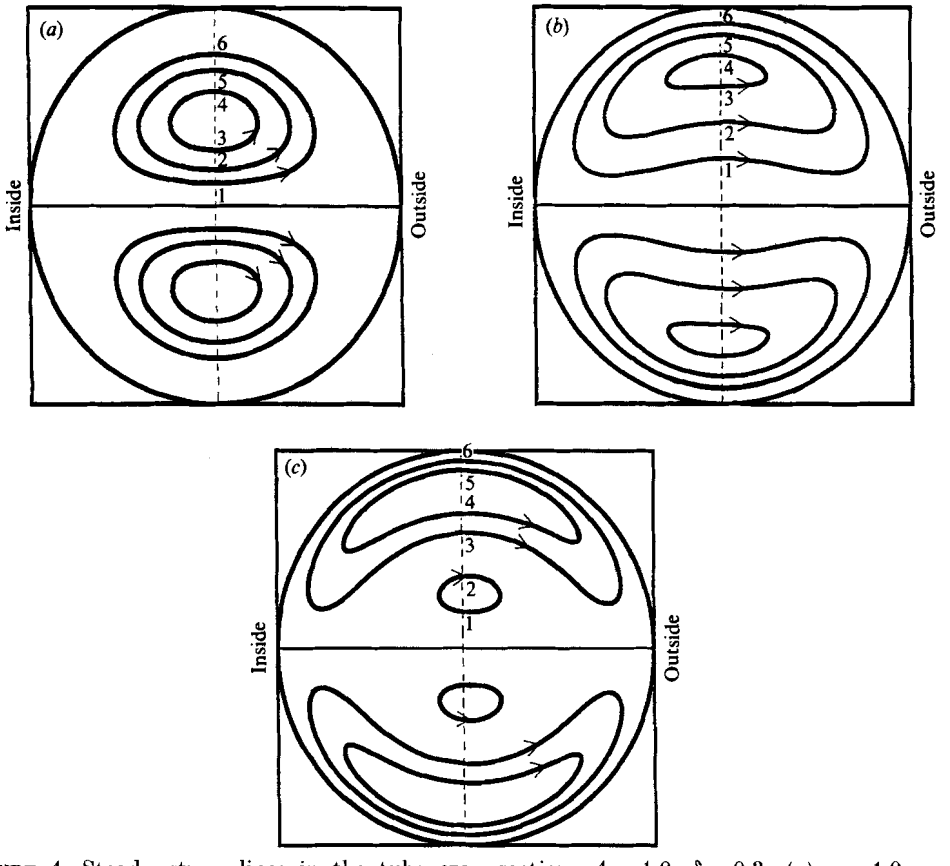

FIGURE 4. Steady streamlines in the tube cross-section. $A = 1.0$, $\delta = 0.3$: (*a*) $\alpha = 1.0$; speed $(u^2+v^2)^{\frac{1}{2}}$ along $\psi = \frac{1}{2}\pi$ is: 1. 0.00636; 2. 0.00545; 3. 0.00336; 4. 0.00326; 5. 0.00481; 6. 0.00510. (*b*) $\alpha = 10.0$; speed $(u^2+v^2)^{\frac{1}{2}}$ along $\psi = \frac{1}{2}\pi$ is: 1. 0.0166; 2. 0.0264; 3. 0.0209; 4. 0.0215; 5. 0.0594; 6. 0.0630. (*c*) $\alpha = 15.0$; speed $(u^2+v^2)^{\frac{1}{2}}$ along $\psi = \frac{1}{2}\pi$ is: 1. 0.00397; 2. 0.00545; 3. 0.0024; 4. 0.0296; 5. 0.0451; 6. 0.0558.

authors, but, again, since we are interested in the transport problem, we seek specific information about the values of α for which these behaviours occur. For example, when $A = 1$ our work and previous work shows that for $\alpha > 11$ the second set of steady cells has already appeared, since the leading-order equations are the same. However, the $O(\delta)$ terms are much weaker for Lyne (1970) and Mullin & Greated (1980) since their equations neglect certain centrifugal terms for simplification of the problem. The effect of this is that their cells are much more centred than those shown here, which are noticeably off-centre. For example, at $\alpha = 10$, the pair of vortices are offset toward the inside wall. At $\alpha = 15$ these vortices are squeezed against the wall, still off-centre to the inside. The new pair of vortices in the core are off-centre to the outside. While the solutions are more difficult to obtain, this illustrates the importance of retaining all of the terms in the equations of motion at each order. Of added significance in terms of transport is that the strength and off-centring of these vortices will mix the solute in a distinctly different way from the vortices predicted by Lyne (1970) and Mullin & Greated (1980). The ramifications of this are discussed in §9.

5. Problem formulation: concentration field

Given the velocity field, transport properties of the solute within the tube may be calculated from the convection–diffusion equation, which governs the transport of a soluble species. In dimensionless form for toroidal coordinates it is given as:

$$C_t + \delta A^2\left(uC_r + \frac{v}{r}C_\psi\right) + \frac{AwC_s}{h} = \alpha^{-2}Sc^{-1}\nabla^2 C, \tag{5.1}$$

where

$$\nabla^2 = \frac{\partial^2}{\partial r^2} + \frac{1}{r}\frac{\partial}{\partial r} + \frac{\cos\psi}{h}\frac{\partial}{\partial r} + \frac{1}{r^2}\frac{\partial^2}{\partial r^2} - \left[\frac{\sin\psi}{rh}\right]\frac{\partial}{\partial\psi} + \frac{1}{h}\frac{\partial^2}{\partial s^2}. \tag{5.2}$$

The dimensionless local concentration, $C(r, \psi, s, \tau)$, is related to its dimensional form, $\overset{*}{C}(\overset{*}{r}, \psi, \overset{*}{s}, \overset{*}{t})$, by the formula $C = (\overset{*}{C} - C_R)/(C_L - C_R)$, given that C_R and C_L are the specified steady concentrations at the tube ends. The velocity field (u, v, w) used here satisfies the Navier–Stokes equations given above. The parameters in the convection–diffusion equation are the same as were used in the momentum and mass conservation equations. The one new parameter appearing here is the Schmidt number, $Sc = \nu/D$, where D is the molecular diffusivity of the solute in the solvent. The boundary conditions selected are no flux at the tube wall,

$$\frac{\partial C}{\partial r} = 0 \quad \text{at } r = 1, \tag{5.3}$$

and the concentration within the tube must be bounded at the centre,

$$C \text{ bounded at } r = 0. \tag{5.4}$$

We impose uniform time-averaged concentrations at the ends of the curved tube such that

$$C^{(s)} = 1 \quad \text{at } s = 0, \quad C^{(s)} = 0 \quad \text{at } s = l, \tag{5.5a, b}$$

where the superscript (s) denotes the steady component of the concentration.

6. Method of solution: concentration field

The appearance of the small parameter δ in the convection–diffusion equation suggests a regular perturbation scheme for the concentration field:

$$C(r,\psi,s,t) = C_0(r,\psi,s,t) + \delta C_1(r,\psi,s,t) + \delta^2 C_2(r,\psi,s,t) + O(\delta^3). \tag{6.1}$$

Substituting equations (3.1a, b) and (6.1) into the convection–diffusion equation gives a linear boundary-value problem at each order of δ. The solution to the leading-order problem is the straight-pipe solution determined by Watson (1983),

$$C_0 = 1 - \frac{s}{l} + [L(r)\,\mathrm{e}^{\mathrm{i}\tau} + \text{c.c.}], \tag{6.2}$$

where $L(r)$ is determined in the same manner as was used to determine the velocity field. The radial dependence of the forcing of the leading-order convection–diffusion equation can be represented as $\Gamma(r) = -\alpha^2 ScA W_0 C_{0s}$ so that

$$L(r) = [l_1 + F_1(\Gamma, Sc^{\frac{1}{2}}\sigma, 0)]J_0(Sc^{\frac{1}{2}}\sigma r) + F_2(\Gamma, Sc^{\frac{1}{2}}\sigma, 0)Y_0(Sc^{\frac{1}{2}}\sigma r), \tag{6.3}$$

where the constant l_1 is determined from the $O(1)$ boundary condition at $r = 1$.

Solving the $O(\delta)$ problem with this same technique gives the solution

$$C_1 = [U_1(r)\,\mathrm{e}^{\mathrm{i}\tau} + U_2(r)\,\mathrm{e}^{3\mathrm{i}\tau} + \text{c.c.}]\cos\psi, \tag{6.4}$$

where
$$U_1 = [l_2 + F_1(\Omega_1, Sc^{\frac{1}{2}}\sigma, 1)]J_1(Sc^{\frac{1}{2}}\sigma r) + F_2(\Omega_1, Sc^{\frac{1}{2}}\sigma, 1)\,Y_1(Sc^{\frac{1}{2}}\sigma r), \tag{6.5a}$$

$$U_2 = [l_3 + F_1(\Omega_2, (3Sc)^{\frac{1}{2}}\sigma, 1)]J_1(3Sc)^{\frac{1}{2}}\sigma r) + F_2(\Omega_2, (3Sc\sigma)^{\frac{1}{2}}, 1)Y_1((3Sc)^{\frac{1}{2}}\sigma r), \tag{6.5b}$$

and $\Omega_1(r)$ and $\Omega_2(r)$ are the radial dependence of the $\mathrm{e}^{\mathrm{i}\tau}$ and $\mathrm{e}^{3\mathrm{i}\tau}$ forcing terms of the $O(\delta)$ convection–diffusion equation, respectively. The constants l_2 and l_3 are determined from the $O(\delta)$ boundary condition at $r = 1$. The solution given in (6.4) can readily be shown to be independent of axial variation.

The $O(\delta^2)$ convection–diffusion equation suggests a solution of the form

$$\begin{aligned} C_2 = {} & [\Delta_1(r)\,\mathrm{e}^{\mathrm{i}\tau} + \Delta_2(r)\,\mathrm{e}^{3\mathrm{i}\tau} + \Delta_3(r)\,\mathrm{e}^{5\mathrm{i}\tau} + \text{c.c.}] \\ & + [\Pi_1(r)\,\mathrm{e}^{\mathrm{i}\tau} + \Pi_2(r)\,\mathrm{e}^{3\mathrm{i}\tau} + \Pi_3(r)\,\mathrm{e}^{5\mathrm{i}\tau} + \text{c.c.}]\sin 2\psi \\ & + [\epsilon_1(r)\,\mathrm{e}^{\mathrm{i}\tau} + \epsilon_2(r)\,\mathrm{e}^{3\mathrm{i}\tau} + \epsilon_3(r)\,\mathrm{e}^{5\mathrm{i}\tau} + \text{c.c.}]\cos 2\psi. \end{aligned} \tag{6.6}$$

Looking ahead to the calculation for the mass flux we note that we must find the component of C_2 which is $\mathrm{e}^{\mathrm{i}\tau}$ dependent and independent of ψ. Therefore we solve only for $\Delta_1(r)$ from (6.6) subject to (5.3) and (5.4), employing our solution technique as before. Upon substitution, the radial dependence of the $\mathrm{e}^{\mathrm{i}\tau}$-periodic, ψ-independent forcing term of the $O(\delta^2)$ equation can be written as $Z(r)$, leading to the solution

$$\Delta_1(r) = [l_4 + F_1(Z, Sc^{\frac{1}{2}}\sigma, 0)]J_0(Sc^{\frac{1}{2}}\sigma r) + F_2(Z, Sc^{\frac{1}{2}}\sigma, 0)Y_0(Sc^{\frac{1}{2}}\sigma r), \tag{6.7}$$

where l_4 is a constant determined from (5.3).

7. Results: concentration field

The oscillatory component of the concentration field through $O(\delta)$ in the plane of curvature is shown for $\tau = \frac{1}{4}\pi$ and various values of α in figure 5(a–b). It is of note here that the concentration profile mimics the appearance of the velocity profile. That is, for large enough α a concentration boundary layer develops near the tube

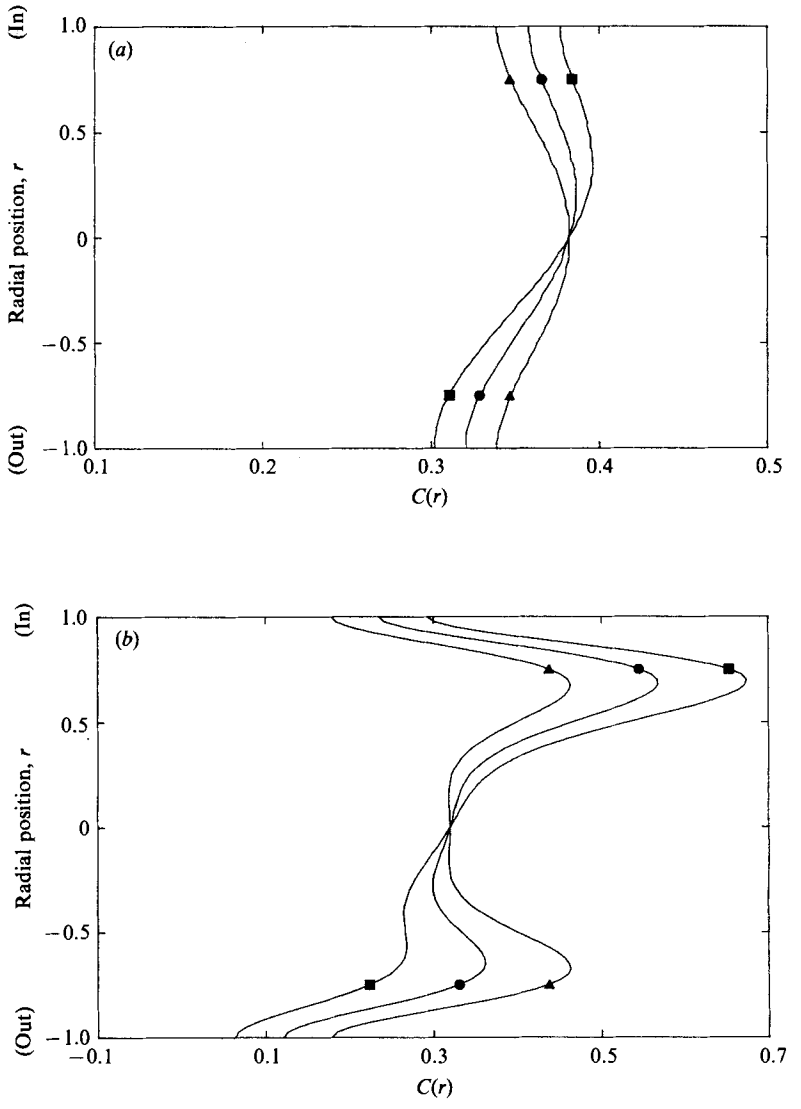

FIGURE 5. Concentration profile in plane of curvature as a function of r. $\tau = \frac{1}{4}\pi$, $Sc = 0.9$, $A = 1.0$. Tubes used are ▲, $\delta = 0$; ●, $\delta = 0.15$; ■, $\delta = 0.3$. (*a*) $\alpha = 1.0$; (*b*) $\alpha = 10.0$.

wall. The concentration is higher near the inside wall and lower near the outside wall, as can be seen from the form of the first correction for the concentration. As we described for the velocity case, we again note the dependence of C_1 on $\cos\psi$ so that we add a correction to the straight-tube case on the outer half of the tube and we subtract that correction from the straight-tube case on the inner half of the tube. For large α the radial-dependence of this correction is negative. A value of 0.9 for the Schmidt number is used for all of these graphs.

8. Mass transport

We are interested in the time-mean longitudinal mass transport through the curved tube under conditions of volume-cycled flow with uniform steady end concentrations. The dimensionless steady axial mass flow rate, m, is expressed by

$$m = \int_{\tau_0}^{\tau_0+2\pi} \int_0^{2\pi} \int_0^1 \left[\alpha^2 A w C - \frac{1}{Sc}\frac{\partial C}{\partial s}\right] r \, \mathrm{d}r \, \mathrm{d}\psi \, \mathrm{d}\tau. \tag{8.1}$$

The dimensional steady axial mass flow rate, with dimensions of mass per unit time, is given by $\overset{*}{m} = mva\Delta\overset{*}{C}$, where $\Delta\overset{*}{C}$ is the difference between the specified steady concentrations at the tube ends. The steady local mass flux, $\overset{*}{q} = \overset{*}{m}/\pi a^2$, in dimensions of mass per unit time per unit cross-sectional tube area, has dimensionless form $q = m/\pi$ where $q = \overset{*}{q}a/v\Delta\overset{*}{C}$. This is independent of the axial coordinate since the tube has uniform cross-section.

Inserting the perturbation solutions to w and C and keeping only the terms which are independent of τ and ψ, since these terms integrate to zero, gives

$$m = 2\pi \int_0^1 \left\{\alpha^2 A[W_0(r)\,\bar{L}(r) + \delta^2 (W_0(r)\,\bar{A}_1(r) + \tfrac{1}{2}[\bar{h}_1(r)\,U_1(r) + \bar{h}_2(r)\,U_2(r)] + \bar{\lambda}(r)\,L(r)) + \text{c.c.}] + \frac{1}{lSc}\right\} r \, \mathrm{d}r, \tag{8.2}$$

where the superscript bar denotes complex conjugate.

9. Results: mass transport

Solutions to (8.2) are provided in figures 6–7. Values of $Sc = 0.9$ and $l = 7.0 + 3.5\ (3)^{\frac{1}{2}}$ are used since they are physiologically reasonable and they allow direct comparison of these results to those in Godleski & Grotberg (1987). When the Womersley parameter is fixed the mass flow rate increases monotonically with A, and the value of δ determines the magnitude of the increase. This is shown in figure 6(a, b) for $\alpha = 2$ and 12, respectively. The enhancement of transport over the straight-tube case can be explained by the fact that as A increases, the effect of the secondary flows due to curvature is to redistribute the soluble material into a concentration profile that mimics or 'overlays' the axial velocity profile. Since the transport is measured by the product of w and C, we find enhancement of transport for the curved tube since more of the soluble contaminant is present in the region of faster axial flow and less of the soluble species is present in the region of slower axial flow. As the curvature of the tube increases, the secondary flows become greater and the distortion of the axial velocity and concentration profiles increases in similar fashion so that transport increases. This is unlike the case of steady flow where the effect of the secondary flows is to distort the concentration profile in a manner not similar to the distortion of the axial velocity profile. The regions of faster flow, in this case, convect less of the soluble species so that the total transport becomes disenhanced from the straight-tube case. Increasing the curvature here means decreasing the transport from that in a straight tube as in Johnson & Kamm (1986).

When the Womersley parameter increases for fixed A we again see an increase in the transport characteristics of curved tubes over straight tubes. This is plotted in figure 7(a). As α becomes larger, fluid elements are subjected to greater centrifuging

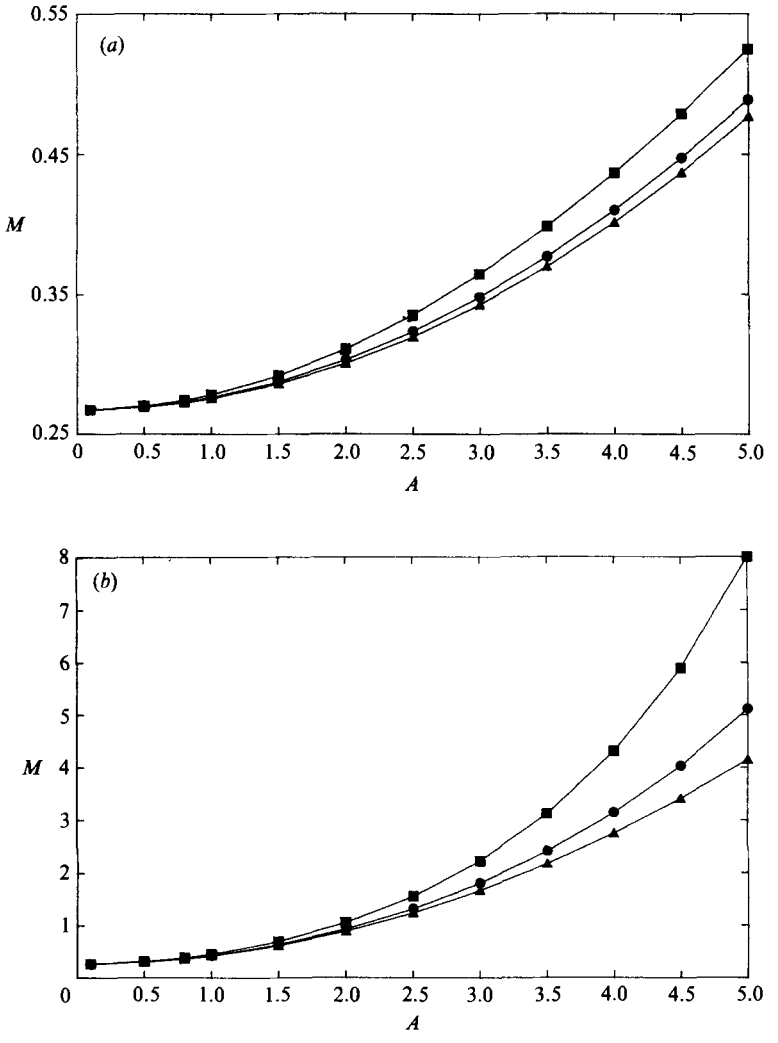

FIGURE 6. Steady mass flow rate as a function of A. $Sc = 0.9$. Tubes used are ▲, $\delta = 0$; ●, $\delta = 0.15$; ■, $\delta = 0.3$. (*a*) $\alpha = 2.0$; (*b*) $\alpha = 12.0$.

and the lateral motions become greater. In essence, we are observing the same effect described above. These larger secondary flows cause distortion of the concentration profile, which mimics the axial velocity profile, resulting in greater mass flux.

As α increases when $A = 5$, the mass transport in a straight tube increases monotonically whereas the mass delivered by the curved tube is enhanced over the straight-tube case and passes through a local maximum. This is depicted in figure 7 (*b*). The enhancement in the curved tube is due to three particular interactions: the interaction of W_0 with C_2; W_1 with C_1; and W_2 with C_0. The transport from these three components is shown in figure 7 (*c*). It is clear that the interaction of W_0 with C_2 dominates the enhancement of transport in the region of the local maximum of figure 7 (*b*). It might be expected that W_0, the fastest component of the axial flow, would convect the greatest amount of mass. However, it is difficult to offer an intuitive description of the behaviour of $A_1(r)\,e^{i\tau} + \text{c.c.}$, the component of C_2 which survives the time integral in the computation of the mass flux. This component is

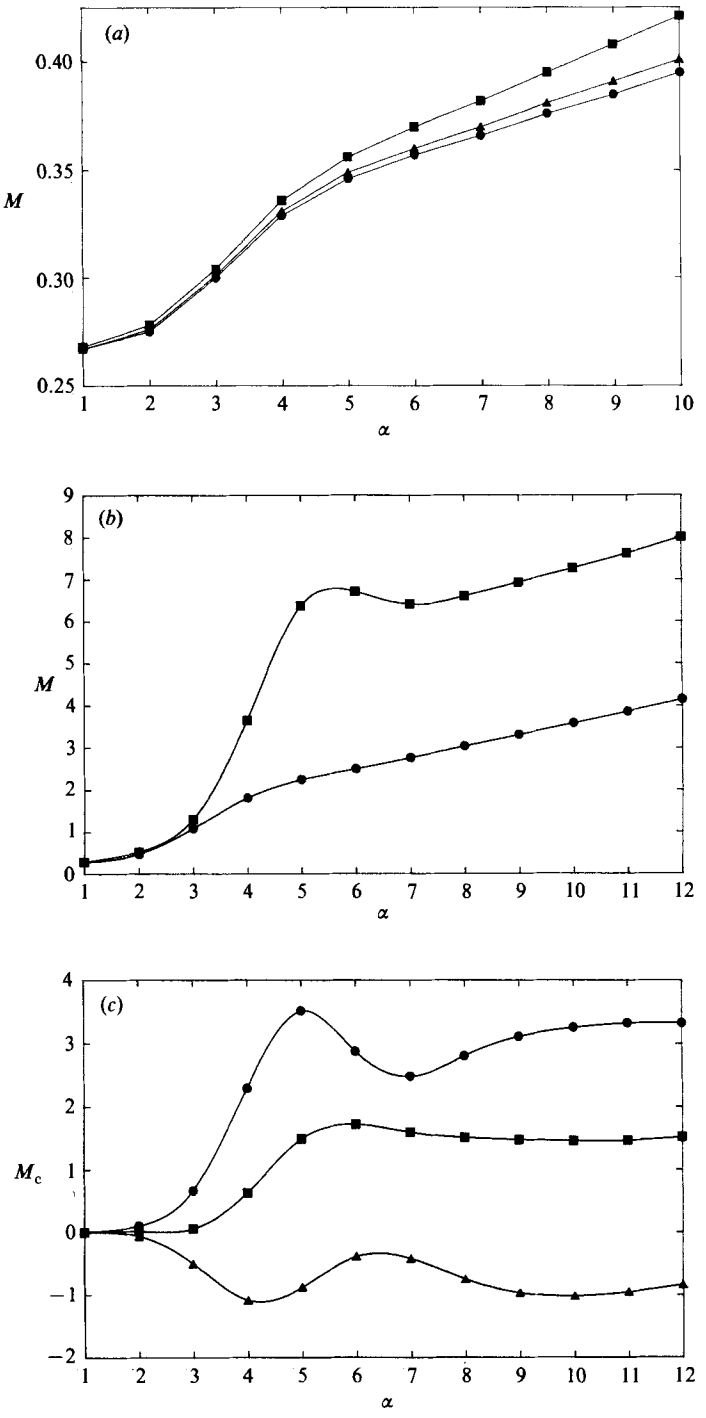

FIGURE 7. (*a*,*b*) Steady mass flow rate as a function of α. $Sc = 0.9$. Tubes used are ●, $\delta = 0$; ▲, $\delta = 0.15$; ■, $\delta = 0.3$. (*a*) $A = 1.0$; (*b*) $A = 5.0$. (*c*) $O(\delta^2)$ contributions to steady mass flow rate as a function of α. $Sc = 0.9$, $A = 5$, $\delta = 0.3$. Interactions are ●, W_0C_2; ■, W_1C_1; ▲, W_2C_0.

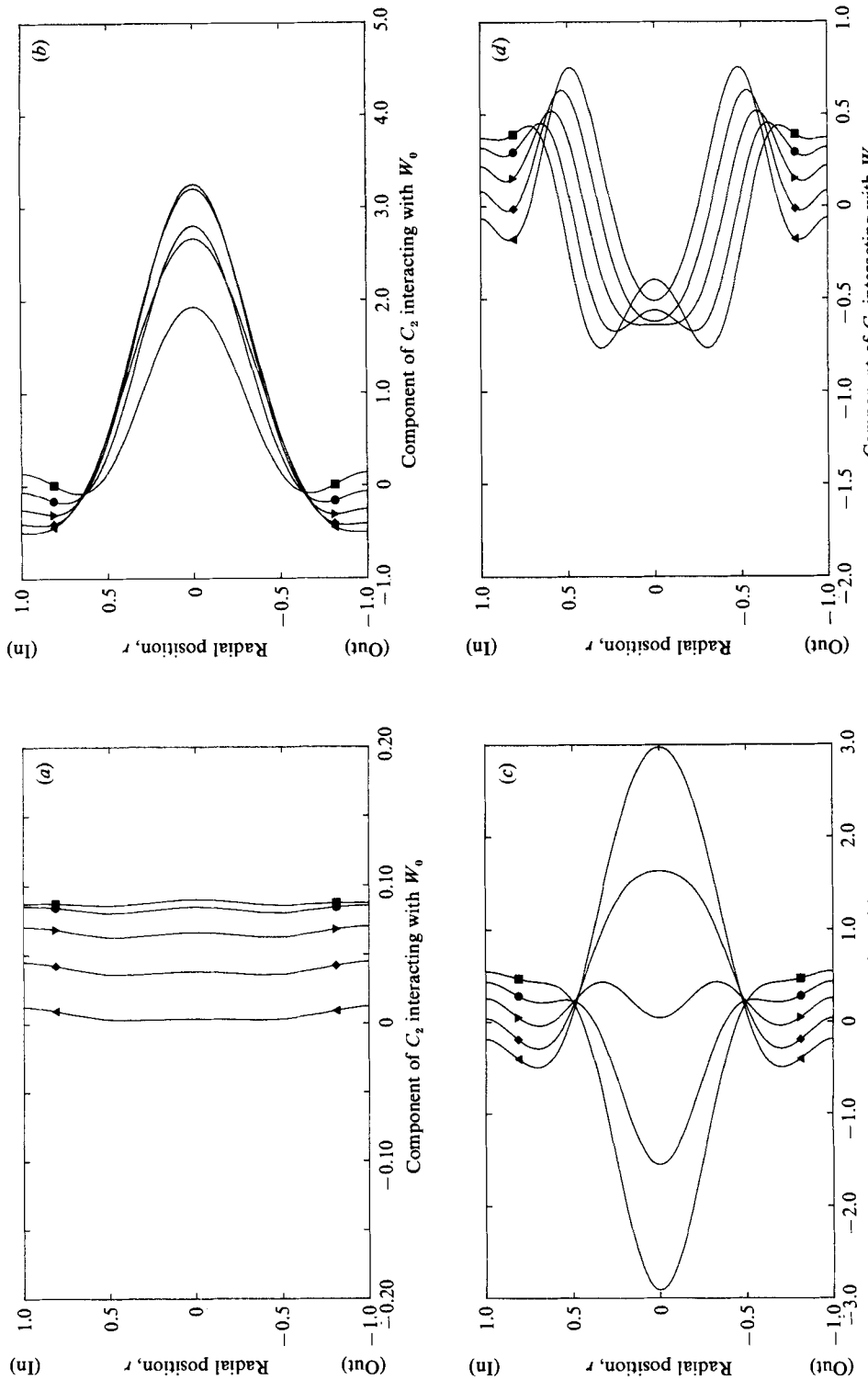

FIGURE 8. Component of C_2 which interacts with W_0 as a function of r, $\delta = 0.3$, $A = 5.0$, $Sc = 0.9$. Phases shown are ■, $\tau = 0$; ●, $\tau = \frac{1}{8}\pi$; ▼, $\tau = \frac{1}{4}\pi$; ◆, $\tau = \frac{3}{8}\pi$; ▲, $\tau = \frac{1}{2}\pi$. (*a*) $\alpha = 2.0$; (*b*) $\alpha = 5.0$; (*c*) $\alpha = 7.0$; (*d*) $\alpha = 10.0$.

graphed at various phases in the cycle in figure 8(*a–d*). For $\alpha = 2$ the concentrations are very small during the cycle, as seen in figure 8(*a*). The mass convected by the interaction of these low concentrations with the axial velocity should therefore be relatively small, and in figure 7(*c*) it is so observed. When $\alpha = 5$, figure 8(*b*) shows that the concentration term is in phase with the leading-order axial velocity. The regions of fastest flow are near the wall, where the concentrations are lowest, but the core flow is carrying highly concentrated fluid. The transport from this interaction is large, as seen in figure 7(*c*). When α is increased to 7, figure 8(*c*) shows this part of the concentration field is out of phase with the axial velocity. The interaction between the two is thus weakened with the resultant transport decreased. As α increases beyond 7, the transport in both the curved and straight tubes increases monotonically. The enhancement is still primarily due to the W_0–C_2 interaction. When $\alpha = 10$, figure 8(*d*) shows that the concentration component has decreased in magnitude. The core flow is slow for large α, while the flow near the wall is quite fast. The region of fastest axial flow convects low concentrations of solute, but this will dominate the convection in the core where the velocities are small. As α increases, the velocity and concentration profiles do not change much in general character, so the enhancement of transport over the straight tube continues to increase, but slowly.

Careful term by term analysis of the ordered Navier–Stokes and convection–diffusion equations showed that while the dimensionless coefficients ($\alpha^2 A^2$) could become quite large in the parameter ranges selected in this analysis, the terms these coefficients multiplied decreased in magnitude such that the products remained $O(1)$. This confirmed that ordering the perturbation sequence in powers of δ was appropriate and that corrections remained small, i.e. $w_0 > \delta w_1 > \delta^2 w_2$ as $\delta \to 0$.

A common method of expressing the enhancement of mass transport due to the interaction of diffusion with convection is by defining an effective diffusivity, $\overset{*}{D}_{\text{eff}}$, as the ratio of the time-mean mass flux to the steady axial concentration gradient. For the model presented here, this ratio is given by $\overset{*}{D}_{\text{eff}} = -\overset{*}{q}/\overset{*}{C}_0'(s)$. In dimensionless form, this becomes

$$D_{\text{eff}} = -\frac{mSc}{\pi C_0'(s)} = \frac{mScl}{\pi}. \tag{9.1}$$

This is independent of the axial coordinate, s, and varies from the calculated mass flow rate, m, by a constant. Therefore, one can see what the effective diffusivity for the curved and straight tubes are directly from figures 6 and 7, which depict the relationship of m with A and α.

10. Discussion

Oscillatory flow in both straight and curved tubes couples axial convection with radial diffusion. Solute convected along a streamline can diffuse radially in the straight tube to regions of faster axial velocity. The net effect is to enhance axial transport over one cycle. In addition to axial convection, solute is convected radially and azimuthally by secondary flows in a curved tube. Solute can cross streamlines by axial, radial or azimuthal diffusion, so the coupling mechanism of diffusion and convection seen (5.1) includes all these effects. The mass flow rate predicted for curved tubes is further enhanced over that of straight tubes for all values of A and α investigated. In a typical ventilator application we can think of fixed A as constant tidal volume and increasing α as increasing breathing frequency. Of particular interest, then, is the transport for the curved tube when $A = 5$. For $2 < \alpha < 5$ there

is a rapid rise in the transport and considerable enhancement over the straight-tube case. In a ventilator application, it is valuable to select breathing frequencies that will optimize gas exchange within a frequency range tolerable to the patient. The model suggests the steep part of the curve in this domain of α as a desirable operating region. As α is increased over the range 5 to 10, however, there is relatively little change in the overall transport, with both a local maximum followed by a local minimum evident. In a clinical setting it is essential to know if the inability to increase gas exchange while increasing breathing frequency is a measure of pathology or a predictable feature of the mass transport characteristics of a normal lung undergoing HFV. Our model indicates that, to the extent that airway curvature is important, this inability could, in fact, be expected.

The effective diffusivity is a convenient method of defining the lumped transport properties for straight tubes. In the curved tube it differs from the mass flowrate by a multiplicative constant; therefore an oscillatory flow in a curved tube enhances the effective diffusivity of a soluble contaminant. This may explain, in part, the experimental results of Paloski *et al.* (1987) where measured transport rates in a branching network of identical straight tubes were greater than those predicted by the straight-tube theory of Watson (1983).

This work was supported by NIH grant HL/GM-30574, the NIH Research Career Development Award HL-01818 and the NSF Presidential Young Investigator Award MEA-8351494 in conjunction with General Motors Corporation, G. D. Searle and Inland Steel. We wish to acknowledge the valuable advice of Dr Gregory Kriegsmann and Dr Michael Borgas.

REFERENCES

BERGER, S. A., TALBOT, L. & YAO, L. S. 1983 Flow in curved pipes. *Ann. Rev. Fluid Mech.* **15**, 461–512.

BERTELSEN, A. F. & THORSEN, L. K. 1982 An experimental investigation of oscillatory flow in pipe bends. *J. Fluid Mech.* **118**, 269–284.

BLENNERHASSETT, P. 1976 Secondary motion and diffusion in unsteady flow in a curved pipe. Ph.D. Thesis, Imperial College, London.

BOHN, D. J., MIYASAKA, K., MARCHAK, E. B., THOMPSON, W. K., FROESE, A. B. & BRYAN, A. C. 1980 Ventilation by high-frequency oscillation. *J. Appl. Physiol.* **48**, 710–716.

BUTLER, W. J., BOHN, D. J., BRYAN, A. C. & FROESE, A. B. 1980 Ventilation by high-frequency oscillation in humans. *Anesth. Analg.* **59**, 577–584.

CHATWIN, P. C. 1975 On the longitudinal dispersion of passive contaminant in oscillatory flows in tubes. *J. Fluid Mech.* **71**, 513–527.

ERDOGAN, M. E. & CHATWIN, P. C. 1967 The effects of curvature and bouyancy on the laminar dispersion of solute in a horizontal tube. *J. Fluid Mech.* **29**, 465–484.

GAVER, D. P. & GROTBERG, J. B. 1986 An experimental investigation of oscillating flow in a tapered channel. *J. Fluid Mech.* **172**, 47–61.

GODLESKI, D. A. & GROTBERG, J. B. 1987 Convection–diffusion interaction for oscillatory flow in a tapered tube. *Trans. ASME* K: *J. Biomech. Engng* (To appear).

GROTBERG, J. B. 1984 Volume-cycled oscillatory flow in a tapered channel. *J. Fluid Mech.* **141**, 249–264.

HASELTON, F. R. & SCHERER, P. W. 1982 Flow visualization of steady streaming in oscillatory flow through a bifurcating tube. *J. Fluid Mech.* **123**, 315–333.

JANSSEN, L. A. M. 1976 Axial dispersion in laminar flow through coiled tubes. *Chem. Engng Sci.* **31**, 215–218.

JOHNSON, M. & KAMM, R. D. 1986 Numerical studies of steady flow dispersion at low Dean number in a gently curving tube. *J. Fluid Mech.* **172**, 329–345.

JOSHI, C. H., KAMM, R. D., DRAZEN, J. M. & SLUTSKY, A. S. 1983 An experimental study of gas exchange in laminar oscillatory flow. *J. Fluid Mech.* **133**, 245–254.

LYNE, W. H. 1970 Unsteady viscous flow in a curved pipe. *J. Fluid Mech.* **45**, 13–31.

MULLIN, T. & GREATED, C. A. 1980 Oscillatory flow in curved pipes. Part 2. The fully developed case. *J. Fluid Mech.* **98**, 397–416.

NIGAM, K. D. P. & VASUDEVA, K. 1976 Influence of curvature and pulsations on laminar dispersion. *Chem. Engng Sci.* **31**, 835–837.

PALOSKI, W. H., SLOSBERG, R. B. & KAMM, R. D. 1987 Effects of gas properties and wave form asymmetry on gas transport in a branching tube network. *J. Appl. Phys.* **62**, 892–901.

SMITH, F. T. 1975 Pulsatile flow in curved pipes. *J. Fluid Mech.* **71**, 15–42.

TAYLOR, G. I. 1953 Dispersion of soluble matter in solvent flowing slowly through a tube. *Proc. R. Soc. Lond.* A **219**, 186–203.

VAN DEN BERG, J. H. M. & DEELDER, R. S. 1979 Measurement of axial dispersion in laminar flow through coiled capillary tubes. *Chem. Engng Sci.* **34**, 1345–1347.

WATSON, E. J. 1983 Diffusion in oscillatory pipe flow. *J. Fluid Mech.* **133**, 233–244.

YAMANE, R., OSHIMA, S., SUDO, K., SUMIDA, M., OKAMOTO, N. & KIZAKI, M. 1985 Study of Oscillatory Flow in Curved Channel. *Bull. JSME* **28**, 428–435.